JACS
JOURNAL OF THE AMERICAN CHEMICAL SOCIETY
Communication
pubs.acs.org/JACS

Atomically Dispersed Ru on Ultrathin Pd Nanoribbons

Jingjie Ge,[†,Δ] Dongsheng He,[‡,Δ] Wenxing Chen,[§] Huanxin Ju,[⊥] Han Zhang,[†] Tingting Chao,[†] Xiaoqian Wang,[†] Rui You,[†] Yue Lin,[†] Yu Wang,[∥] Junfa Zhu,[⊥] Hai Li,[#] Bin Xiao,[†] Weixin Huang,[†] Yuen Wu,[†] Xun Hong,*[,†] and Yadong Li*[,†,§]

[†]Center of Advanced Nanocatalysis (CAN) and Department of Chemistry, University of Science and Technology of China, Hefei, Anhui 230026, China

[‡]Materials Characterization and Preparation Center (MCPC), South University of Science and Technology of China, Shen-zhen, Guangdong 518055, China

[§]Department of Chemistry and Collaborative Innovation Center for Nanomaterial Science and Engineering, Tsinghua University, Beijing 100084, China

[⊥]National Synchrotron Radiation Laboratory (NSRL), University of Science and Technology of China, Hefei, Anhui 230029, China

[∥]Shanghai Synchrontron Radiation Facilities, Shanghai Institute of Applied Physics, Chinese Academy of Science, Shanghai 201800, China

[#]Key Laboratory of Flexible Electronics (KLOFE) & Institute of Advanced Materials (IAM), Jiangsu National Synergetic Innovation Center for Advanced Materials (SICAM), Nanjing Technology University, Nanjing, Jiangsu 211816, China

Supporting Information

ABSTRACT: We report a one-pot synthesis of atomically dispersed Ru on ultrathin Pd nanoribbons. By using synchrotron radiation photoemission spectroscopy (SRPES) and extended X-ray absorption fine structure (EXAFS) measurements in combination with aberration corrected high-resolution transmission electron microscopy (HRTEM), we show that atomically dispersed Ru with content up to 5.9% was on the surface of the ultrathin nanoribbon. Furthermore, the ultrathin Pd/Ru nanoribbons could remarkably prohibit the hydrogenolysis in chemoselective hydrogenation of C═C bonds, leading to an excellent catalytic selectivity compared with commercial Pd/C and Ru/C.

The properties of noble metals may greatly differ from their bulk as the size reduces to subnanometer or atomic level.[1] Recently, atomically dispersed noble metal on a support has attracted increasing attention because of their fascinating properties and applications in catalysis.[2] A number of studies have shown that atomically dispersed noble metal supported on zeolites,[3,4] carbon,[5] or metal oxides[6−8] can efficiently catalyze various important reactions by maximally utilizing the atom efficiency. In particular, atomically dispersed noble metal embedded in other noble metal substrates exhibits enhanced catalytic properties due to the synergistic effects of the isolated atoms and metal substrates.[9−15] For example, atomically dispersed Pd atoms on a Cu(111) single crystal surface lower the energy barrier to both hydrogen uptake and desorption from the Cu surface and the bimetallic catalyst, which was shown to be active for selective hydrogenation of styrene and acetylene.[10]

Although the atomically dispersed noble metal embedded in host metal was shown to be attractive alternative catalyst to traditional bimetallic catalyst, the synthesis is a challenging task. Generally, the isolated metal on metal substrate is prepared via electron beam evaporators under ultrahigh vacuum or alloying low density (below 1 wt %) single atoms with metal substrate.[9−15] These synthetic methods require special experimental setup and multistep reaction conditions and thus are restricted to large amount production. Moreover, to increase the loading density of the isolated metal is still challenging. In our work, a novel ultrathin nanostructure that is composed of 5.9 wt % atomically dispersed Ru atoms on ultrathin Pd nanoribbons (Pd/Ru nanoribbons) was synthesized by a one-pot wet chemistry process. The Pd/Ru nanoribbons exhibited excellent catalytic performance with extraordinary high chemoselectivity in the selective hydrogenation of allyl benzyl ether without any hydrogenolysis.

In a typical synthesis, palladium(II) 2,4-pentanedionate ($Pd(acac)_2$, 0.032 mmol, 10.0 mg), poly(vinylpyrrolidone) (PVP, 32 mg) were dissolved in 2 mL of *N*,*N*-dimethylacetamide (DMA) and 4 mL of deionized water solution by magnetic stirring under 1 atm atmosphere of CO. The mixture was heated from room temperature to 100 °C within 20 min and kept for 2 h under magnetic stirring. Then the $RuCl_3{\cdot}xH_2O$ solution (0.24 mmol, 62 mg/mL, 800 μL) was injected into the mixture solution and the mixture kept at 100 °C for another 30 min.

The obtained nanoribbons with length of 93.8 ± 17.8 nm and width of 10.2 ± 2.3 nm are confirmed with the transmission electron microscopy (TEM) image (Figure 1a) and the corresponding size distribution histograms (Figure S1). The high-angle annular dark-field scanning transmission electron microscopy (HAADF-STEM) images and the scanning transmission electron microscopy energy-dispersive X-ray spectroscopy (STEM-EDX) elemental mapping reveal that the nanoribbon is composed of Pd and Ru (Figure 1b,c).

Received: September 2, 2016
Published: October 14, 2016

DOI: 10.1021/jacs.6b09246
J. Am. Chem. Soc. 2016, 138, 13850−13853

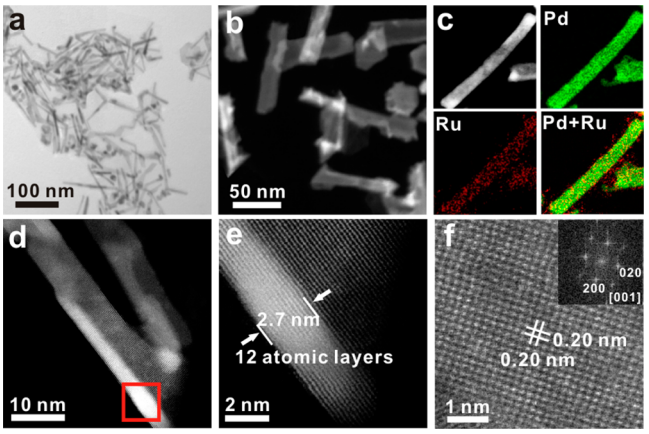

Figure 1. (a) TEM and (b) HAADF-STEM images of the Pd/Ru nanoribbons. (c) HAADF-STEM image of a Pd/Ru nanoribbon and the corresponding STEM-EDX elemental mapping. Aberration-corrected HAADF-STEM images of (d) a side view of the Pd/Ru nanoribbons, (e) the folded area marked by red squares in (d), showing a thickness of 2.7 nm, and (f) the atomic resolution HAADF-STEM image of a nanoribbon and the corresponding FFT pattern (inset).

Quantitative EDX spectrum of the nanoribbons shows that the atom ratio of Ru and Pd is about 1:16 (Figure S2), consistent with the result obtained by inductively coupled plasma and atomic emission spectrum (ICP-AES). The thickness of a nanoribbon is estimated to be about 2.7 nm (~12 atomic layers) from the aberration-corrected HAADF-STEM images (Figure 1d,e) of the folded edge. Atomic force microscopy (AFM) image (Figure S3) shows that the thickness of the nanoribbons is 3.7 nm, which is about 1 nm thicker than that estimated by the aberration-corrected HAADF-STEM image due to the capping of PVP. The lattice fringes of 0.20 nm is corresponding to the {200} plane distance of Pd (Figure 1f). Fast Fourier transform (FFT) pattern can be well interpreted by the face-centered cubic (fcc) phase. The X-ray diffraction (XRD) pattern of the Pd/Ru nanoribbons shows three pronounced reflection peaks at 2θ = 40.01°, 46.59°, and 68.09°, corresponding to the fcc Pd(111), (200), and (220) reflections, respectively (Figure S4).

The synchrotron radiation photoemission spectroscopy (SRPES) spectra of Pd 3d and Ru 3d as shown in Figure 2a,b were measured with photon energies of 400, 500, 600, and 1486.6 eV, respectively, at the BL11U beamline in the National Synchrotron Radiation Laboratory (NSRL) in Hefei, China. For SRPES measurements, the nanoribbons were deposited on

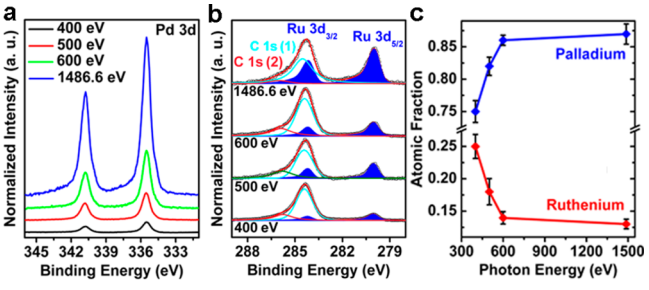

Figure 2. (a) Pd 3d and (b) Ru 3d SRPES spectra of the Pd/Ru nanoribbons with different photon energies. (c) Dependence of Ru and Pd atomic fractions of the Pd/Ru nanoribbons as a function of photon energy.

silicon wafer and treated with argon ion beam sputtering to minimize the influence of the PVP capped on the surface. As shown in Figure 2a, peaks at 340.8 and 335.5 eV can be assigned to Pd $3d_{3/2}$ and Pd $3d_{5/2}$ of metallic Pd^0, respectively. Ru $3d_{3/2}$ signals overlap with the C 1s signals from PVP around 285 eV, and the component of Ru could be obtained by the spectrum decomposition. The peaks at 280.1 eV can be assigned to Ru $3d_{5/2}$ of metallic Ru^0 (Figure 2b). The peak areas were calibrated by the beam flux and photoionization cross-section at the corresponding photon energy. Figure 2c shows Ru and Pd atomic fractions of the Pd/Ru nanoribbons. The atomic fraction of Ru decreases from 0.25 to 0.12 when the photoenergy increases from 400 to 1486.8 eV, indicating that Ru is on the surface of the Pd/Ru nanoribbons.[16]

The structure of the Pd/Ru nanoribbons was further investigated by the X-ray absorption near-edge structure (XANES) and the extended X-ray absorption fine structure (EXAFS). Pd nanosheets obtained before adding $RuCl_3 \cdot xH_2O$ were used as the reference material (Figure S5). As shown in Figure 3a, the Pd K-edge XANES spectrum of the Pd/Ru

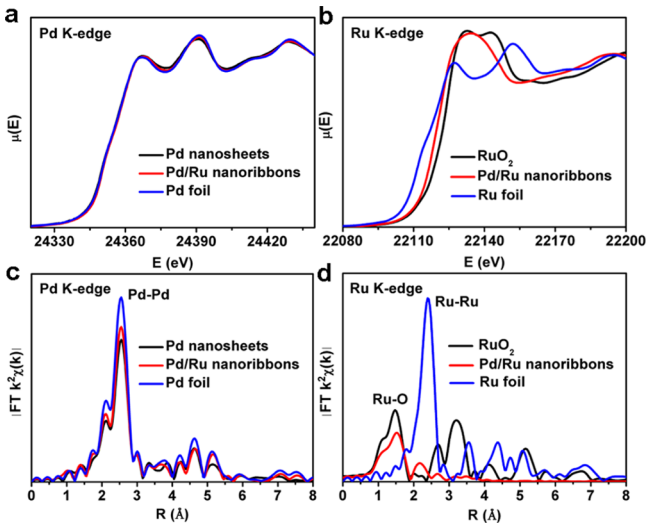

Figure 3. XANES spectra of the Pd/Ru nanoribbons for (a) Pd K-edge and (b) Ru K-edge. Fourier transformed (FT) k^2-weighted $\chi(k)$-function of the EXAFS spectra for (c) Pd K-edge and (d) Ru K-edge.

nanoribbons is similar to that of Pd foil and Pd nanosheets, indicating the metal state of Pd. Figure 3b shows the Ru K-edge of the Pd/Ru nanoribbons with reference materials RuO_2 and Ru foil. The XANES of the Pd/Ru nanoribbons shows higher energy absorption edge than that of Ru foil reference and lower energy than that of RuO_2, suggesting the oxidized $Ru^{\delta+}$ rather than Ru^{4+} or Ru^0. Figures 3c and S6–S8 show the Fourier-transformed EXAFS spectra of Pd K-edge for Pd/Ru nanoribbons, Pd nanosheets, and Pd foil. For the Pd/Ru nanoribbons, the intensity of the peak at 2.55 Å, which is assigned to the first shell of Pd–Pd scattering, is lower than that of Pd foil and higher than that of Pd nanosheets. The Pd–Pd coordination number from curving fittings for Pd/Ru nanoribbons, Pd nanosheets, and Pd foil are 11, 10, and 12, respectively (Table S1). Figures 3d and S9–S10 show the Fourier-transformed EXAFS spectra of Ru K-edge for Pd/Ru nanoribbons and RuO_2. The notable peak at 1.52 Å for the Pd/Ru nanoribbons was from the Ru–O contribution. The absence of Ru–Ru or Ru–Pd peaks indicated that atomically

DOI: 10.1021/jacs.6b09246
J. Am. Chem. Soc. 2016, 138, 13850–13853

dispersed Ru is on the surface and oxidized during the ex situ EXAFS experiment. The coordination number of Ru−O is 5.2 ± 0.6, close to that of RuO_2 (Table S2).

Time-dependent experiments were conducted to understand the formation mechanism of atomically dispersed Ru on ultrathin Pd nanoribbons. Figure S11a schematically illustrates the shape evolution of the Pd/Ru nanoribbons. First, ultrathin Pd nanosheets were synthesized (Figure S11b) similarly to those for synthesizing ultrathin Pd nanosheets by using CO as a surface confining agent.[17,18] However, the obtained nanosheets were not completely flat where the edge (~3 nm in width) is thicker than the center (Figure S12a,b). After 8 equiv of $RuCl_3 \cdot xH_2O$ aqueous solution was added, the morphology changed significantly within 1 min. Nanoribbons as well as some irregular shape nanostructures with bends and kinks were observed (Figure S11c). The STEM image of a kinked nanostructure (inset of Figure S11c) suggested that the Pd/Ru nanoribbons were formed by breaking off ultrathin Pd nanosheets. The EDX mapping confirmed that Pd/Ru nanoribbons were formed with a reaction of 1 min after $RuCl_3 \cdot xH_2O$ solution was added (Figure S13). In our previous study, we found that monolayer Ru atoms could be deposited on the surface of octahedral Pd nanoparticles via underpotential deposition process.[19] However, the deposited monolayer is imperfect and defective sites are widely observed.[19−21] To understand why atomically dispersed Ru atoms deposited on Pd surface, we performed a quantitative analysis of the HAADF-STEM image of the intermediate Pd nanostructure using a model-based analysis method.[22] The estimated number of atom within each column is displayed in Figure S12c (see the Supporting Information for more details), which shows that the surface of the Pd was not atomically flat, thus isolated Ru atoms might locate at steps or edges on the ultrathin Pd nanoribbons.

The atomically dispersed Ru atoms on ultrathin Pd nanoribbons might show great promise for catalysis due to the high surface area and the synergistic effect between the atomically dispersed Ru and the host Pd. Figure 4a schematically illustrates the performance of chemoselective hydrogenation of allyl benzyl ether (**1a**), a reference compound that represents typical hydroxyl protecting group with hydrogenation of other reducible functionalities smooth in the synthetic chemistry. Using the obtained Pd/Ru nanoribbons as catalyst, (propoxymethyl)benzene (**2a**) was obtained exclusively in the hydrogenation of allyl benzyl ether (Figure 4a, from **1a** to **2a**), while the hydrogenolysis of (propoxymethyl)-benzene was inhibited (Figure 4a, from **2a** to **2b**). Promisingly, the conversion of **1a** was highly up to 100% and 99% chemoselectivity of **2a** were obtained (Figures 4b,c and S14). The durability of the Pd/Ru nanoribbons was also conducted, and the catalytic activity and chemoselectivity were maintained excellently after 5 cycles (Figure S15). Control experiments using commercial Ru/C (Figure S16a) and Pd/C (Figure S16b) catalysts were performed at the same conditions, respectively. The chemoselective hydrogenation of **1a** catalyzed by commercial Ru/C scarcely proceeded (Figures 4b,c and S14). For commercial Pd/C, the consumption rate of **1a** was slightly faster than that of the Pd/Ru nanoribbon catalyst (Figure 4b). However, the hydrogenolysis of *O*-benzyl protecting group was further proceeded and the over-hydrogenated product 1-propanol (**2b**) was obtained (Figures 4c and S14). As known, the dissociation adsorption of H_2 is often the rate-limiting step in hydrogenation and hydrogenolysis reactions. For the Pd/Ru nanoribbon catalyst, decorating the host Pd with atomically dispersed Ru could decrease the binding energy of hydrogen and reaction intermediate compared to pure Pd or Ru metal, which could prohibit the overhydrogenation.[23−25] The unique catalytic mechanism is similar to the single atoms alloys catalysts for selective hydrogenation reactions.[10,11,13]

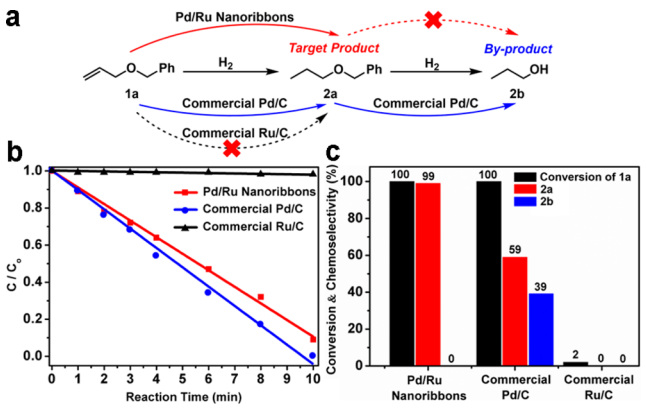

Figure 4. Catalytic behaviors of the ultrathin Pd/Ru nanoribbons. (a) Schematic illustration of the catalytic chemoselective hydrogenation of allyl benzyl ether. (b,c) Allyl benzyl ether consumption rate, (b) the conversion of allyl benzyl ether, and (c) chemoselectivity of (propoxymethyl)benzene catalyzed by the Pd/Ru nanoribbons, commercial Pd/C, commercial Ru/C, respectively. See Supporting Information for more details.

In summary, we reported the preparation of a novel bimetallic Pd/Ru nanoribbons with length of 93.8 ± 17.8 nm, width of 10.2 ± 2.3 nm, and thickness of ~2.7 nm. The SRPES and EXAFS results indicate that isolated Ru atoms were atomically dispersed on the surface of the Pd nanoribbons. Quantitative EDX spectrum and ICP-AES results illustrate that the nanoribbons contain 5.9 wt % Ru. The bimetallic nanoribbons were formed by breaking off ultrathin Pd nanosheets followed by the deposition of isolated Ru species on the steps or edges of the nonatomically flat Pd nanosheets. The obtained ultrathin nanoribbons exhibit high catalytic performance in chemoselective hydrogenation of alkene functionality without any hydrogenolysis of the *O*-benzyl protecting group. We believe that the versatile route for the synthesis of the Pd/Ru nanoribbons can be estimated to improve the design of novel bimetallic catalysts on an atomic level.

■ ASSOCIATED CONTENT

Supporting Information

The Supporting Information is available free of charge on the ACS Publications website at DOI: 10.1021/jacs.6b09246.

Detailed experimental procedures; HAADF-STEM images; EDX spectra, AFM image; XRD data and fitting results of the EXAFS spectra of atomically dispersed Ru on ultrathin Pd nanoribbons (PDF)

■ AUTHOR INFORMATION

Corresponding Authors

*hongxun@ustc.edu.cn

*ydli@mail.tsinghua.edu.cn

Author Contributions

[Δ]J.G. and D.H. contributed equally to this work.

DOI: 10.1021/jacs.6b09246
J. Am. Chem. Soc. 2016, 138, 13850−13853

Notes

The authors declare no competing financial interest.

■ ACKNOWLEDGMENTS

This work was supported by the Fundamental Research Funds for the Central Universities (WK2060190042), National Natural Science Foundation of China (21571169), State Key Project of Fundamental Research for Nanoscience and Nanotechnology (2011CB932401 and 2011CBA00500), and National Key Basic Research Program of China (2012CB224802).

■ REFERENCES

(1) Corma, A.; Concepción, P.; Boronat, M.; Sabater, M. J.; Navas, J.; Yacaman, M. J.; Larios, E.; Posadas, A.; López-Quintela, M. A.; Buceta, D.; Mendoza, E.; Guilera, G.; Mayoral, A. *Nat. Chem.* **2013**, *5*, 775.
(2) Flytzani-Stephanopoulos, M.; Gates, B. C. *Annu. Rev. Chem. Biomol. Eng.* **2012**, *3*, 545.
(3) Ding, K.; Gulec, A.; Johnson, A. M.; Schweitzer, N. M.; Stucky, G. D.; Marks, L. D.; Stair, P. C. *Science* **2015**, *350*, 189.
(4) Aydin, C.; Lu, J.; Liang, A. J.; Chen, C.-Y.; Browning, N. D.; Gates, B. C. *Nano Lett.* **2011**, *11*, 5537.
(5) Yan, H.; Cheng, H.; Yi, H.; Lin, Y.; Yao, T.; Wang, C. L.; Li, J. J.; Wei, S. Q.; Lu, J. L. *J. Am. Chem. Soc.* **2015**, *137*, 10484.
(6) Qiao, B. T.; Wang, A.; Yang, X.; Allard, L. F.; Jiang, Z.; Cui, Y.; Liu, J.; Li, J.; Zhang, T. *Nat. Chem.* **2011**, *3*, 634.
(7) Liu, P. X.; Zhao, Y.; Qin, R.; Mo, S.; Chen, G.; Gu, L.; Chevrier, D. M.; Zhang, P.; Guo, Q.; Zang, D.; Wu, B. H.; Fu, G.; Zheng, N. *Science* **2016**, *352*, 797.
(8) Qiao, B.; Liang, J.-X.; Wang, A.; Xu, C.-Q.; Li, J.; Zhang, T.; Liu, J. J. *Nano Res.* **2015**, *8*, 2913.
(9) Zhang, H.; Watanabe, T.; Okumura, M.; Haruta, M.; Toshima, N. *Nat. Mater.* **2012**, *11*, 49.
(10) Kyriakou, G.; Boucher, M. B.; Jewell, A. D.; Lewis, E. A.; Lawton, T. J.; Baber, A. E.; Tierney, H. L.; Flytzani-Stephanopoulos, M.; Sykes, E. C. H. *Science* **2012**, *335*, 1209.
(11) Lucci, F. R.; Liu, J. L.; Marcinkowski, M. D.; Yang, M.; Allard, L. F.; Flytzani-Stephanopoulos, M.; Sykes, E. C. H. *Nat. Commun.* **2015**, *6*, 8850.
(12) Liu, J.; Lucci, F. R.; Yang, M.; Lee, S.; Marcinkowski, M. D.; Therrien, A. J.; Williams, C. T.; Sykes, E. C. H.; Flytzani-Stephanopoulos, M. *J. Am. Chem. Soc.* **2016**, *138*, 6396.
(13) Aich, P.; Wei, H.; Basan, B.; Kropf, A. J.; Schweitzer, N. M.; Marshall, C. L.; Miller, J. T.; Meyer, R. *J. Phys. Chem. C* **2015**, *119*, 18140.
(14) Pei, G. X.; Liu, X. Y.; Wang, A.; Lee, A. F.; Isaacs, M. A.; Li, L.; Pan, X.; Yang, X.; Wang, X.; Tai, Z.; Wilson, K.; Zhang, T. *ACS Catal.* **2015**, *5*, 3717.
(15) Tierney, H. L.; Baber, A. E.; Kitchin, J. R.; Sykes, E. C. H. *Phys. Rev. Lett.* **2009**, *103*, 246102.
(16) Tao, F.; Grass, M. E.; Zhang, Y. W.; Butcher, D. R.; Renzas, J. R.; Liu, Z.; Chung, J. Y.; Mun, B. S.; Salmeron, M.; Somorjai, G. A. *Science* **2008**, *322*, 932.
(17) Siril, P. F.; Ramos, L.; Beaunier, P.; Archirel, P.; Etcheberry, A.; Remita, H. *Chem. Mater.* **2009**, *21*, 5170.
(18) Huang, X.; Tang, S.; Mu, X.; Dai, Y.; Chen, G.; Zhou, Z.; Ruan, F.; Yang, Z.; Zheng, N. *Nat. Nanotechnol.* **2011**, *6*, 28.
(19) Ge, J.; He, D.; Bai, L.; You, R.; Lu, H.; Lin, Y.; Tan, C.; Kang, Y.-B.; Xiao, B.; Wu, Y.; Deng, Z.; Huang, W.; Zhang, H.; Hong, X.; Li, Y. *J. Am. Chem. Soc.* **2015**, *137*, 14566.
(20) Sasaki, K.; Naohara, H.; Choi, Y. M.; Cai, Y.; Chen, W.-F.; Liu, P.; Adzic, R. R. *Nat. Commun.* **2012**, *3*, 1115.
(21) Yang, S.; Lee, H. *ACS Catal.* **2013**, *3*, 437.
(22) Van Aert, S.; Batenburg, K. J.; Rossell, M. D.; Erni, R.; Van Tendeloo, G. *Nature* **2011**, *470*, 374.
(23) Greeley, J.; Mavrikakis, M. *Nat. Mater.* **2004**, *3*, 810.
(24) Greeley, J.; Mavrikakis, M. *J. Phys. Chem. B* **2005**, *109*, 3460.
(25) Ramos, M.; Minniti, M.; Díaz, C.; Farías, D.; Miranda, R.; Martín, F.; Martíneza, A. E.; Busnengo, H. F. *Phys. Chem. Chem. Phys.* **2013**, *15*, 14936.

DOI: 10.1021/jacs.6b09246
J. Am. Chem. Soc. 2016, 138, 13850−13853